

## Article

# Determination of Geographic Origin of Turquoise by Combining Laser Ablation Inductively Coupled Plasma Mass Spectrometry Analysis and Chemometrics

Shuoyun Tong<sup>1,2,3,\*</sup> , Guodong Chen<sup>1</sup>, Weikang Hu<sup>1,2,4</sup>, Shiyang Pan<sup>1,2</sup>, Dan Zhu<sup>2,4</sup>, Shuang Liu<sup>2,4</sup>, Li Lu<sup>2,4</sup>, Shunchao Zhou<sup>2,4</sup> and Wanfeng Zhou<sup>2,5,\*</sup>

<sup>1</sup> Key Laboratory of Gold Mineralization Processes and Resource Utilization, Ministry of Natural Resources, Shandong Provincial Key Laboratory of Metallogenic Geological Process and Resource Utilization, Jinan 250013, China; hwksky@126.com (W.H.); psy1583@163.com (S.P.)

<sup>2</sup> Key Laboratory of Rare Mineral, Ministry of Natural Resources, Hubei Geological Research Laboratory, Wuhan 430034, China; sunrisezd@163.com (D.Z.); fuerry@126.com (S.L.); luli73@126.com (L.L.); superman18631@163.com (S.Z.)

<sup>3</sup> Wuhan Center of China Geological Survey, Wuhan 430205, China

<sup>4</sup> Hubei Provincial Jewelry and Jade Quality Supervision and Inspection Center, Wuhan 430034, China

<sup>5</sup> Guizhou Central Laboratory of Geology and Mineral Resources, Guiyang 550018, China

\* Correspondence: tongshuoyun@163.com (S.T.); zhouwanfeng730721@163.com (W.Z.)

**Abstract:** Microsampling elemental analysis is widely used for gemstone and mineralogy traceability. Using laser ablation inductively coupled plasma mass spectrometry combined with chemometrics, the contents of 56 elements in turquoise samples from 5 distinct producing areas in 3 nations were measured. An origin identification model for turquoise samples from various producing areas was established through random forest importance analysis, principal component analysis, and linear discriminant analysis. When combined with random forest importance screening, the traceability efficiency of principal component analysis is significantly improved. Moreover, by taking 48 elements as characteristic variables and introducing them into the discriminant model, a Fisher discriminant model for identifying the origin of turquoise was successfully established. The effective element fingerprint information of turquoise species is closely related to the species origin, and the accuracy of cross-validation reaches 99.5%, demonstrating the feasibility of the proposed model for the identification of the origin of turquoise samples.

**Keywords:** turquoise; chemometrics; origin; laser ablation inductively coupled plasma mass spectrometry



**Citation:** Tong, S.; Chen, G.; Hu, W.; Pan, S.; Zhu, D.; Liu, S.; Lu, L.; Zhou, S.; Zhou, W. Determination of Geographic Origin of Turquoise by Combining Laser Ablation Inductively Coupled Plasma Mass Spectrometry Analysis and Chemometrics. *Minerals* **2023**, *13*, 1338. <https://doi.org/10.3390/min13101338>

Academic Editor: Petrus J Le Roux

Received: 28 July 2023

Revised: 3 October 2023

Accepted: 13 October 2023

Published: 19 October 2023



**Copyright:** © 2023 by the authors. Licensee MDPI, Basel, Switzerland. This article is an open access article distributed under the terms and conditions of the Creative Commons Attribution (CC BY) license (<https://creativecommons.org/licenses/by/4.0/>).

## 1. Introduction

Turquoise, which has attracted attention since ancient times for its beautiful and decorative appearance, featured prominently in the rise of early civilizations, and has maintained a pivotal role in the tradition-steeped inheritance and spiritual tenets of societies, even to this day [1,2]. The economic potential of turquoise and its deposits have garnered widespread international attention, spurring many research and development efforts [3]. Composed of copper aluminum phosphate, turquoises in their natural state tend to exhibit common impurities derived from isomorphism or secondary mineral infiltration [4]. Consumers have been increasingly drawn to high-quality products sourced from specific regions, which command premium prices for items deemed genuine [5]. The main producing areas of turquoise are Iran, United States, China, Egypt, Armenia, Australia, Afghanistan, Russia, Chile, Peru, and South Africa. The most famous source of Iranian turquoise is the Neyshabur turquoise mine, and it is one of the main sources of high-quality turquoise in the world [6]. In addition, China holds a distinguished status as a leading producer of this valuable mineral, boasting the world's largest deposit [7]. Considering its equally important archaeological significance, the development of a reliable and precise

approach to tracing the geographical origins of turquoise continues to hold great academic significance [8–10].

Based on the element compositions, chemometric techniques for geographic origin identification have been widely applied in different fields [11–15]. For example, this technique was employed to predict the geographic origin of wines through the detection of its mineral elements [16–18]. Also, the trace elements and stable isotopes in fruit juices were used to trace the variety and geographic origins of the fruits [19,20]. Moreover, this technique was applied to identify the source of perfumes by detecting elements in the packaging glass [21]. In the domain of jade identification and its origin tracing, discriminant analysis combining trace mineral elements enabled the provenance zoning of chrysotile jadeite, and linear discriminant analysis of trace element data was helpful to differentiate olivine and nephrite from different regions [22–25].

In the field of gemology, Laser Ablation Inductively Coupled Plasma Mass Spectrometry (LA-ICP-MS) has emerged as a widely accepted technique for determining both major and trace element concentrations in different materials [26,27]. The key advantage of LA-ICP-MS is its ability to inflict minimal sample damage, thereby causing relatively low external damage to gemstones [28]. Researchers have employed LA-ICP-MS in a number of studies to identify and trace the geographic origins of gemstones by analyzing their constituent elements. Specifically, LA-ICP-MS has been successfully implemented in the multi-element analyses of minerals, including ruby, sapphire, diamond, topaz, precious corals, and emerald, aiming for mineral origin identification and differentiation [29–35]. Combined with linear discriminant analysis, LA-ICP-MS has an effective ability for source division on nephrite and demantoid garnets [30,31]. When using a nonlinear machine learning algorithm, the geographical source of emerald was distinguished blindly [32]. Besides, canonical discriminant analysis has achieved results for identifying agate and chalcedony in Cambodia and Thailand [33]. In this study, multi-element compositions in turquoise samples from five different regions were analyzed by LA-ICP-MS. Through the utilization of chemometrics and statistical analyses, the samples were classified successfully to their respective sources. Chemometrics was employed to validate the contribution of each variable to the model and distinguish between different sample categories. When combining different analytical methods samples from different sources, a reliable, robust, and sensitive protocol was established for partitioning turquoise from different localities. Moreover, by utilizing the linear discriminant method in conjunction with characteristic trace elements, a high level of accuracy was achieved in distinguishing turquoise samples from different sources.

## 2. Materials and Methods

### 2.1. Reagents and Materials

Argon (99.999%), nitrogen (99.999%), and helium (99.999%) were purchased from Huaxing Industrial Technology Co. (Wuhan, China). De-ionized water ( $>18\text{ M}\Omega$ ) was purified by a Millipore system (Merck Millipore Inc., Billerica, MA, USA). International standard reference materials of NIST-610, BCR-2G, BIR-1G, and BHVO-2G were used for daily tuning and data correction. Analytical pure ethanol (99.99%) was purchased from Sinopharm Reagent (Shanghai, China).

### 2.2. Instrument

The micro-morphology and phase composition of the target minerals were analyzed by a LEICA DM2500P micropolariscope, a ZEISS Sigma 300 high-resolution field emission scanning electron microscope (FE-SEM), and a Bruker X Flash 6/60 X-ray energy spectrometer (EDS) under the conditions of an accelerated voltage of 20 kV, high vacuum mode, working distance of 5–8 mm.

Major and trace element analyses were conducted by LA-ICP-MS at the Key Laboratory of Rare Mineral, Ministry of Natural Resources, Hubei Geological Research Laboratory, Wuhan. Detailed operating conditions for the laser ablation system and the ICP-MS

instrument, and data reduction processes were the same as described by Liu et al. [26,27]. Multi-elemental analyses were performed on an Agilent 7700 (Agilent Technologies Inc., Santa Clara, CA, USA) in combination with a 193 nm ArF excimer laser ablation system (GeoLas 2005, Lambda Physik, Göttingen, Germany). Daily tuning was performed to achieve maximum sensitivity over the whole mass range while minimizing the oxide (~0.5%) and doubly charged (~0.1%) ratio.

Helium was used as the carrier gas. Argon was used as the make-up gas and mixed with the carrier gas via a T-connector before entering the ICP. Nitrogen was added to the central gas flow (Ar + He) of the Ar plasma to improve the detection limit and measurement precision (Hu et al., 2008a). Each analysis incorporated a background acquisition of approximately 15–20 s (gas blank) followed by 40 s of data acquisition from the sample. The Agilent MassHunter was utilized for the acquisition of individual analysis. Elemental content was calibrated against multiple reference materials (BCR-2G, BIR-1G and BHVO-2G) without applying internal standardization. To ensure the smooth running of the matrix normalization calibration, 56 isotopes were measured, including  $^7\text{Li}$ ,  $^9\text{Be}$ ,  $^{11}\text{B}$ ,  $^{23}\text{Na}$ ,  $^{25}\text{Mg}$ ,  $^{27}\text{Al}$ ,  $^{29}\text{Si}$ ,  $^{31}\text{P}$ ,  $^{39}\text{K}$ ,  $^{42}\text{Ca}$ ,  $^{45}\text{Sc}$ ,  $^{47}\text{Ti}$ ,  $^{51}\text{V}$ ,  $^{53}\text{Cr}$ ,  $^{55}\text{Mn}$ ,  $^{57}\text{Fe}$ ,  $^{59}\text{Co}$ ,  $^{60}\text{Ni}$ ,  $^{63}\text{Cu}$ ,  $^{66}\text{Zn}$ ,  $^{71}\text{Ga}$ ,  $^{72}\text{Ge}$ ,  $^{75}\text{As}$ ,  $^{85}\text{Rb}$ ,  $^{88}\text{Sr}$ ,  $^{89}\text{Y}$ ,  $^{91}\text{Zr}$ ,  $^{93}\text{Nb}$ ,  $^{95}\text{Mo}$ ,  $^{107}\text{Ag}$ ,  $^{111}\text{Cd}$ ,  $^{118}\text{Sn}$ ,  $^{121}\text{Sb}$ ,  $^{133}\text{Cs}$ ,  $^{137}\text{Ba}$ ,  $^{139}\text{La}$ ,  $^{140}\text{Ce}$ ,  $^{141}\text{Pr}$ ,  $^{143}\text{Nd}$ ,  $^{147}\text{Sm}$ ,  $^{151}\text{Eu}$ ,  $^{157}\text{Gd}$ ,  $^{159}\text{Tb}$ ,  $^{163}\text{Dy}$ ,  $^{165}\text{Ho}$ ,  $^{166}\text{Er}$ ,  $^{169}\text{Tm}$ ,  $^{173}\text{Yb}$ ,  $^{175}\text{Lu}$ ,  $^{178}\text{Hf}$ ,  $^{181}\text{Ta}$ ,  $^{182}\text{W}$ ,  $^{208}\text{Pb}$ ,  $^{209}\text{Bi}$ ,  $^{232}\text{Th}$ , and  $^{238}\text{U}$ . The preferred values of element concentrations for the USGS reference glasses were obtained from the GeoReM database (<http://georem.mpch-mainz.gwdg.de/> (accessed on 8 January 2023)). Off-line selection and integration of background and analyte signals, time drift correction, and quantitative calibration were performed by data processing software ICPMSDataCal 10.7 software. Quantitative correction was also performed by ICPMSDataCal 10.7 software.

Laser ablation was performed with a spot size of 44  $\mu\text{m}$ , a repetition rate of 7 Hz, and an energy density of 5.5  $\text{J}/\text{cm}^2$ . ICP-MS was performed with a radio frequency power of 1450 w, a sample depth of 6.0 mm, and a nebulizer gas flow of 1.10  $\text{L min}^{-1}$ . According to the ideal chemical formula of turquoise  $\text{CuAl}_6(\text{PO}_4)_4(\text{OH})_8 \cdot 4\text{H}_2\text{O}$  [36], in which the theoretical value of  $\text{H}_2\text{O}$  was calculated as 17.7% wt.%, the element concentrations in each zone were calculated based on the sum of all the determined metal oxides to 82.3% with ICPMSDataCal 10.7 software [37].

### 2.3. Samples and Sampling

To ensure the authenticity and source of turquoise samples, a total of 183 turquoise samples were selected by the Hubei Provincial Jewelry and Jade Quality Supervision and Inspection Center. These samples were commercially available and were procured from three countries and five distinct turquoise-producing regions, including Hubei, Anhui, and Shanxi provinces in China, Mongolia, and the Sleeping Beauty mine in the United States (see Table 1). The sampling area by LA-ICP-MS on the sample is tiny, so it is essential to choose a representative ablation area [38,39]. The samples were carefully polished to expose a smooth plane, fixed in the sample pool with soft plasticine, and kept horizontal.

**Table 1.** Sample information.

| Group | Sample | Site Name       | Country       | Quantity |
|-------|--------|-----------------|---------------|----------|
| 1     | AK     | Ankang          | China         | 33       |
| 2     | MAS    | Maanshang       | China         | 58       |
| 3     | SMR    | Sleeping beauty | United States | 26       |
| 4     | WM     | Mongolia        | Mongolia      | 33       |
| 5     | ZS     | Zhushan         | China         | 33       |

The turquoise samples in this study from different sampling areas were mostly pure blue or green inevitably mixed with carbonaceous material, limonite, secondary quartz, kaolinite, allophane, and other clay minerals; the elemental composition is closely related to the genesis, which was consistent with existing research [7]. In terms of coloration,

turquoise can be blue, blue-green, yellow-green, yellow-brown, brown, reddish brown, and white. The turquoise samples in this study are basically blue or green, the overall structure is relatively loose, and the weathering degree of the samples also varies.

The samples were polished and photographed under a microscope. Some samples were a pure and dense blue color, while others contained mineral impurities, including clay minerals and iron-containing minerals. The microphotographs and backscattered images of random sample from different locations are shown in Figure 1. Because of the involvement of Fe, V, and U elements, the samples show different pure blue, blue-green, and green colors. Elemental composition determined by EDS on the flat surface conformed to the composition characteristics of turquoise (see Table S1), and other minerals such as kaolinite, variscite, pyrite, iron-containing minerals, and clay minerals are occasionally seen.

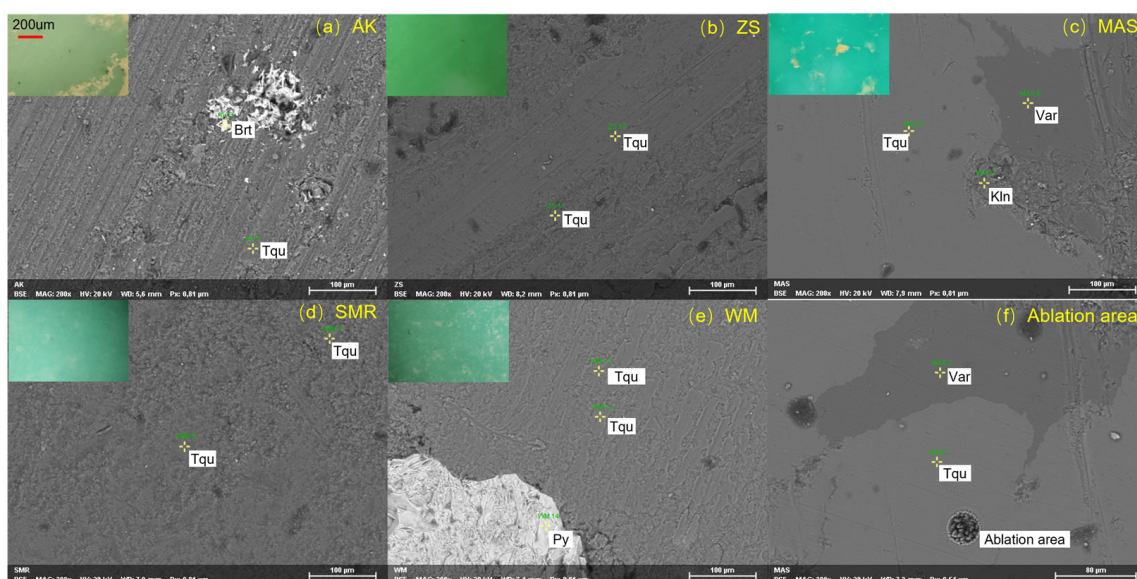


**Figure 1.** Microphotographs and backscattered images from different locations: (a) Ankang, (b) Zhushan, (c) Maanshang, (d) Sleeping beauty, (e) Mongolia, (f) example of ablation area. Mineral abbreviations: Tqu—Turquoise, Brt—Barite, Var—Variscite, Kln—Kaolinite, Py—Pyrite.

The elemental composition analysis was performed by using single-point ablation mode, wherein the samples from each group were uniformly ablated from blue or green colored sections using a laser ablation microscope to ensure that the representativeness of the sample content was maximized. Even for specimens with noticeably associated minerals, uniform blue or green colored sections were accurately selected for testing under a microscope; see Figure 1f. All the ablation areas of each sample were clean surfaces with visual uniform color. Most of the ablation beam accurately fell on turquoise minerals, which can be accurately selected by visual inspection through the microscope camera installed in the laser device. In addition, we confirmed the elemental composition data sets of ablation areas (Section 3.1).

#### 2.4. Statistical Analysis

The statistical calculations for the data were performed using SPSS version 26.0 and Matlab version R2019b. ANOVA was performed on each element; elements were excluded from principal component analysis (PCA) calculation when there was no significant difference ( $p > 0.05$ ) among them.

In order to reduce the dimensionality and to describe all the variability of the entirety data set utilizing fewer variables, principal component analysis (PCA) was utilized. The first principal component (PC1) describes the maximum possible variation and the second principal component (PC2) accounts for the second most, and so on.

Random forest (RF) feature importance selection was used to filter feature element variables. PCA was used again to reduce the dimensions of data and to select characteristic principal components, to further analyze the differences in the elemental composition in separate regions.

Furthermore, the linear discriminant analysis (LDA) model was constructed for additional classification to evaluate whether turquoise from different locations could be statistically separated on the basis of elemental composition that was notably different across regions. Under the “leave-one-out” procedure, a cross-validation test was utilized to assess the robustness of the classification model. Each example in this test was categorized using the functions derived from all cases other than that case, and the classification’s reliability was recalculated by comparing the results to what was already known. The first three discriminant function scores (F1, F2, and F3) were pairwise-crossing plotted to express the sample separation from different regions.

### 3. Results and Discussion

#### 3.1. Multi-Elemental Concentration

Turquoise is a copper aluminophosphate (theoretical chemical formula  $\text{CuAl}_6(\text{PO}_4)_4(\text{OH})_8 \cdot 4\text{H}_2\text{O}$ ). Among 183 samples, the P content (averaged  $119,784 \text{ mg kg}^{-1}$ ) was found to be the highest; Al (averaged  $81,317 \text{ mg kg}^{-1}$ ) the second, and Cu (averaged  $78,754 \text{ mg kg}^{-1}$ ) the third.

Box charts are a statistical method to display the distribution of data; the height of the box reflects the fluctuation of data to some extent. The box diagrams for the P, Al, and Cu elemental concentrations in turquoise samples from different localities are shown in Figure 2. The samples from the Sleeping Beauty mining area were found to contain highest amounts of copper, whereas the samples in Mongolia had the highest amounts of phosphorus. In general, the distributions of these three elements in samples from various producing areas were relatively concentrated, but showed some variations in element contents. In the outlier dots, the samples were still mainly composed of P, Al, and Cu, but when Al was relatively high, the contents of P and Cu decreased correspondingly. In all samples, the sum contents of the three elements reaches a dynamic balance. Although the theoretical chemical formula of turquoise defines the theoretical contents of P, Al, and Cu, the substitution of associated minerals and isomorphism may affect the distribution of the constituent elements.

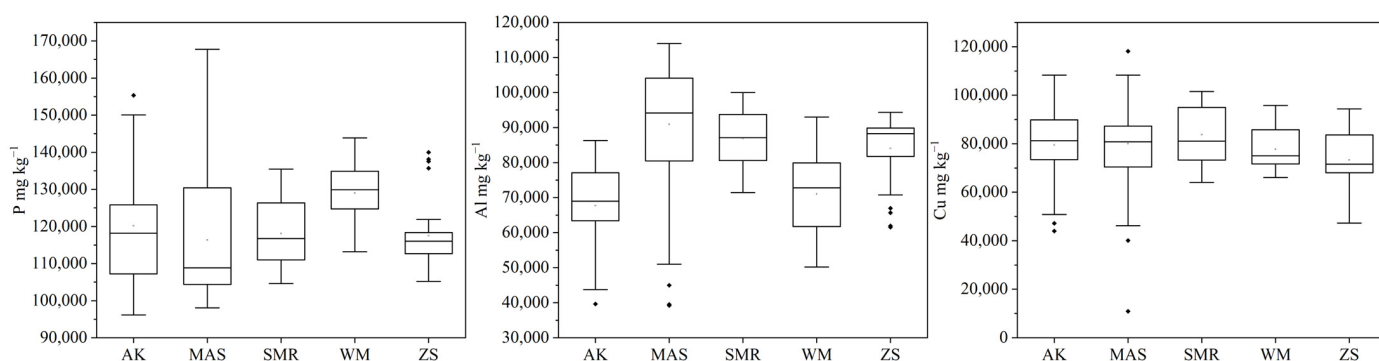


**Figure 2.** Concentrations of elements P, Al, and Cu in turquoise samples from different localities.

The concentrations of elements in turquoise samples from the five producing areas were found in the order  $\text{P} > \text{Al} > \text{Cu} > \text{Fe} > \text{Zn} > \text{Si} > \text{Ca} > \text{As} > \text{K} > \text{Ba} > \text{Na} > \text{Cr} > \text{Ti} > \text{V}$ . Among the five different producing areas, the samples from Ankang, China, contained the highest concentrations of Be, B, V, Fe, Ni, As, Cd, and U, and the samples from Maanshan, China, contained the highest concentrations of Al, Si, Sc, Mn, Co, La and Ce. The samples from the Sleeping Beauty mining area contained the highest concentrations of Na, K, Ca, Cu, Ge, Rb, Y, Ag, Sn, Cs, Pr, Nd, Sm, Eu, Gd, Tb, Dy, Ho, Er, Tm, Yb, Lu, Hf, Ta, W, Bi, and Th. The samples from Mongolia contained the highest concentrations of P, Sr, Ba, and Pb.

While the samples from Zhushan, China, contained the highest concentrations of Li, Mg, Ti, Cr, Zn, Ga, Zr, Nb, Mo, and Sb.

Furthermore, the average contents of 57 elements in 5 regions were calculated, respectively, and the characteristic fingerprint marked by the index on the ordinate is shown in Figure 3. It is worth noting that the rare earth contents in the Sleeping Beauty mining area were particularly high.

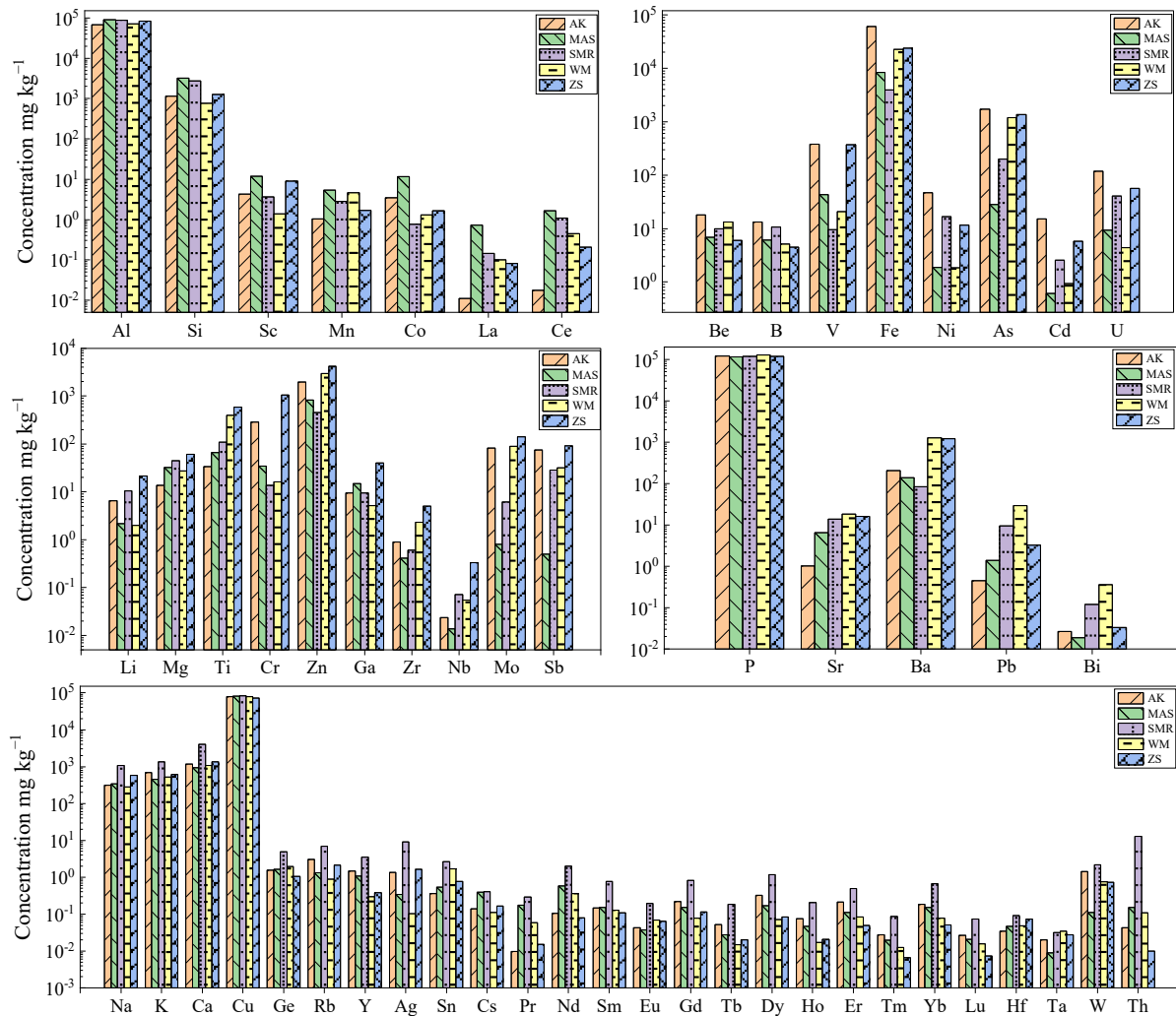


Figure 3. The characteristic fingerprint of the 57 elements in 5 producing areas.

### 3.2. Principal Component Analysis

Principal component analysis, a multivariate statistical method, is one of the most commonly used dimensionality reduction methods. A set of variable data that may be correlated is transformed into a set of linearly uncorrelated variables by orthogonal transformation, and the transformed variables are called principal components. Its purpose is to convert high-dimensional data into low-dimensional data on the premise of less “information loss”, thus reducing the amount of calculation.

ANOVA (analysis of variance) was applied to the obtained data and showed that there was no significant difference ( $p > 0.05$ ) among the elements of Cu, Ag, Cd, Cs, La, Ce, Pr, and Hf in turquoise from different locations. After excluding these elements, 48 elements in turquoise obtained from different habitats were analyzed by principal component analysis.

Using 183 groups of data and 48 variables in each group for dimensionality reduction analysis, the eigenvalues of the first 13 principal components are greater than 1, and the cumulative variance contribution rate of the first 3 principal components is 50.48%. The explanatory power of principal components PC1, PC2, and PC3 of the total variance are

24.80%, 15.36%, and 10.32%, respectively, and 49.53% of the information cannot be found in the first three principal components.

According to the load proportion (Figure 4), elements such as Na, K, Ca, Ge, Rb, Y, Sn, Ta, Th, and rare earth elements account for a large proportion in first principal component, which is consistent with the information on SMR samples in the fingerprint of Figure 3. Li, Mg, Ti, Cr, Ga, Zr, Nb, Mo, and Sb account for a large proportion in the second principal component, which is consistent with the information on ZS samples in the fingerprint. Be, B, V, Fe, Ni, As, and U account for a large proportion of the third principal component, which is consistent with the information of AK sample in fingerprint; P, Sr, Pb, and Bi account for a large proportion of the fourth principal component, which is consistent with the WM sample information in the fingerprint; Na, Mg, Al, Si, Sc, Mn, and Co have a large load in the fifth principal component, which is consistent with the information on MAS samples, SMR samples, and ZS samples in the fingerprint.

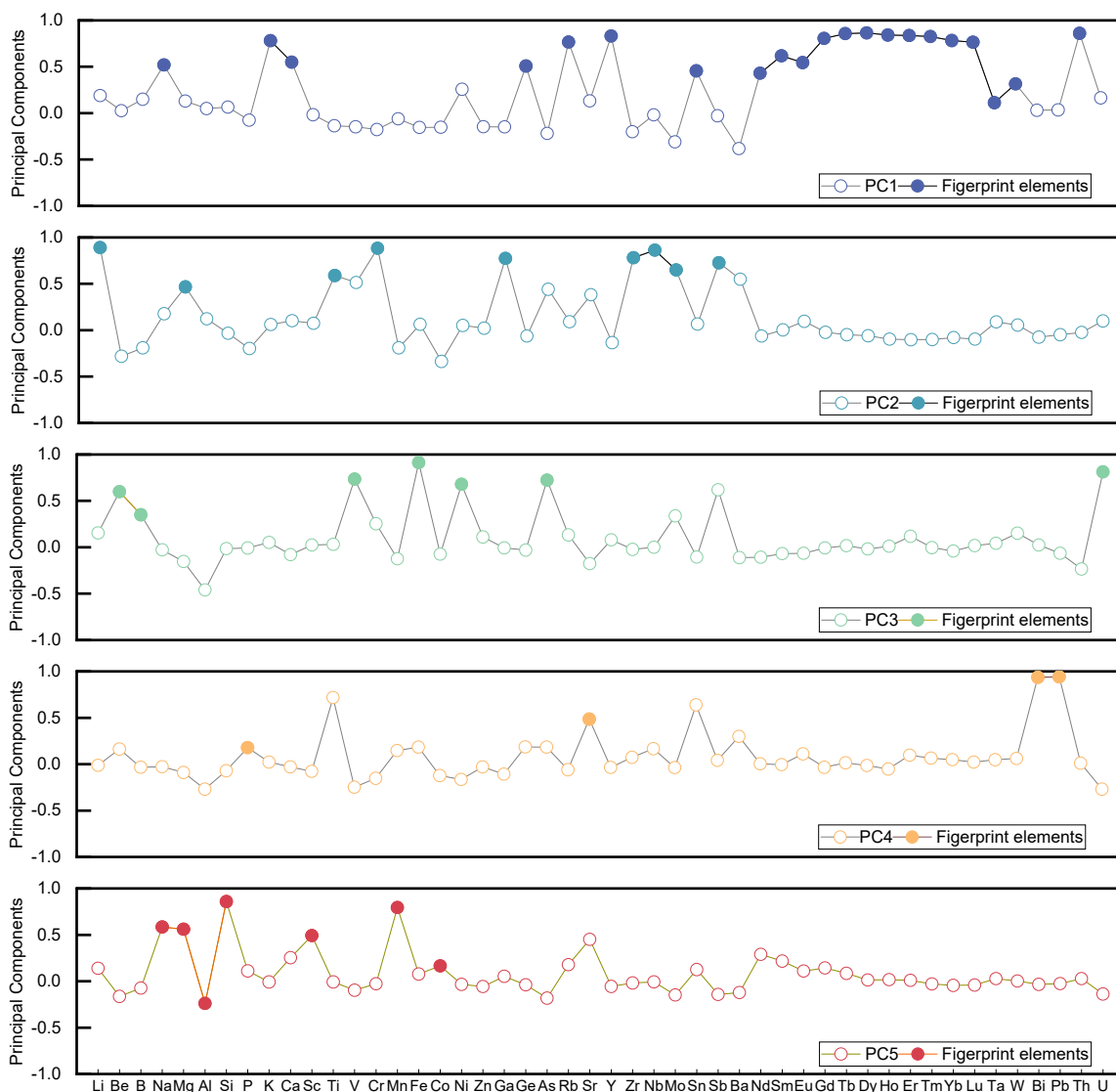
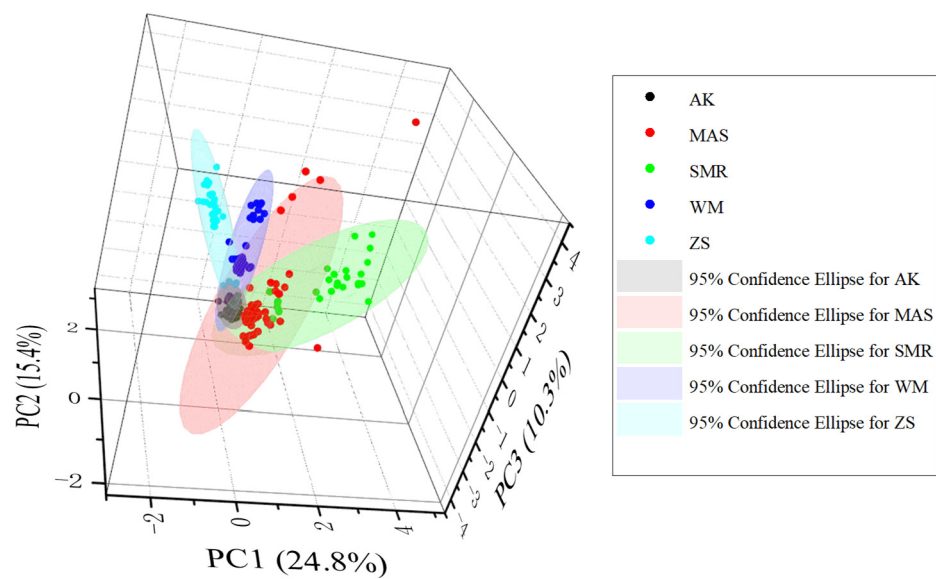


Figure 4. Correspondence between principal components and fingerprint elements.

The distribution of mineral elements from different producing areas presents a certain law. In order to facilitate intuitive analysis, the first three principal components were extracted in a scatter plot (Figure 5). The partition information on samples from different producing areas cannot be clearly distinguished from the plot, and further variable extraction is needed.



**Figure 5.** Principal component analysis results of 48 elemental variables.

**3.3. Combined Variable Selection Based on Random Forest Importance Analysis and Principal Component Analysis**

Random forest is a machine learning algorithm that generates a large number of decision trees through randomly selected training samples and variable subsets, and uses decision trees to predict the results [40–42]. The initial data were 56 sets, through the RF method, the importance of independent variables was analyzed, the number of decision trees was 200, and the number of leaf nodes was 20. The greater the feature importance value, the more important the variable.

In order to screen variables for more effective principal component analysis, the explanatory variance rate of principal components was comprehensively considered in the importance screening, and finally the variables with characteristic importance of >0.036 were screened for principal component analysis (Table 2).

**Table 2.** The variance contribution rate of principal components (PC) before and after importance screening analysis.

| RF     | PC | Eigenvalue | Percentage of Variance (%) | Cumulative (%) |
|--------|----|------------|----------------------------|----------------|
| Before | 1  | 12.39      | 22.13                      | 22.13          |
|        | 2  | 7.42       | 13.26                      | 35.38          |
|        | 3  | 6.28       | 11.22                      | 46.60          |
| After  | 1  | 5.09       | 50.92                      | 50.92          |
|        | 2  | 1.84       | 18.44                      | 69.37          |
|        | 3  | 1.32       | 13.17                      | 82.54          |

In this study, the concentrations of 10 elements (V, Cr, Fe, As, Mo, Sb, Ba, W, Pb, U) measured by LA-ICP-MS were examined by PCA. Utilizing the criterion that characteristic values should exceed the value of 1 and cumulative variance contribution rates should exceed 80%, we achieved six principal component factors through extraction and rotation factors. The total contribution rate of 82.535% indicates that the experimental data effectively capture the original information.

The first principal component is mainly composed of As, Sb, V, Mo, and Cr elements. The second principal component is mainly composed of the element Ba. The third principal component is mainly composed of Fe, W, and Pb elements (Figure 6). These three principal components were used to analyze the contribution of the principal components of samples from different origins. Overall, turquoise samples from different origins exhibit a significant

difference in the contributions to the principal components that can be clearly distinguished; this result has certain significance in guiding the distinction of turquoise from different sites.

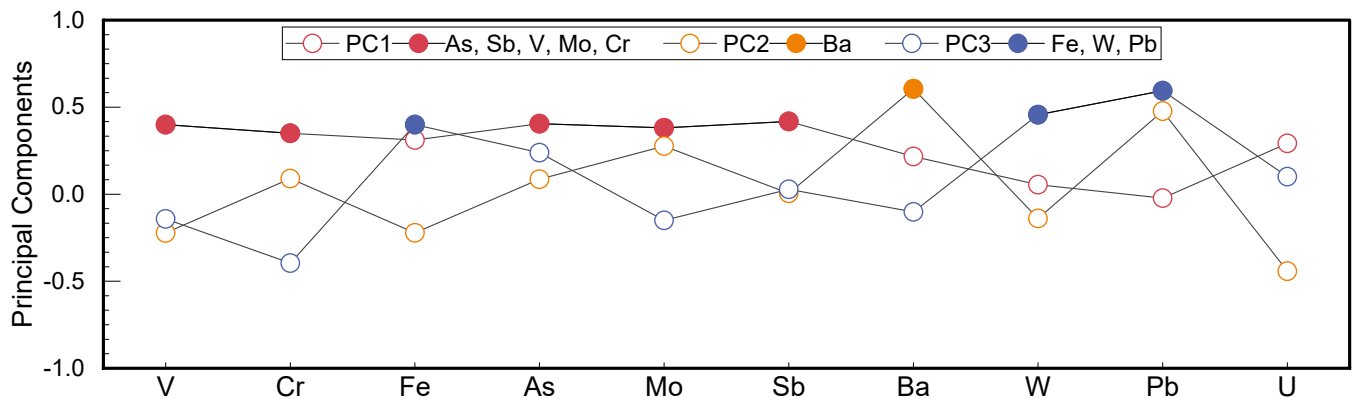


Figure 6. Elemental composition of principal component after RF selection.

Compared with the principal component analysis chart with 48 elements as variables (Figure 7), the scatter charts of PC1–PC2, PC1–PC3, and PC2–PC3 have been significantly improved for the division of producing areas by plotting the principal component scores of 10 variables screened by random forest importance analysis. The samples from Ankang, Mongolia, and Zhushan can be distinguished by PC1–PC2, and the samples from Maan-shan and Sleeping Beauty overlap. In essence, unsupervised principal component analysis cannot reliably distinguish five different origins of turquoise samples. In order to further improve the discrimination accuracy of samples from different origins, another multivariate statistical method was used to obtain more effective results of geographical origin traceability of turquoise [43].

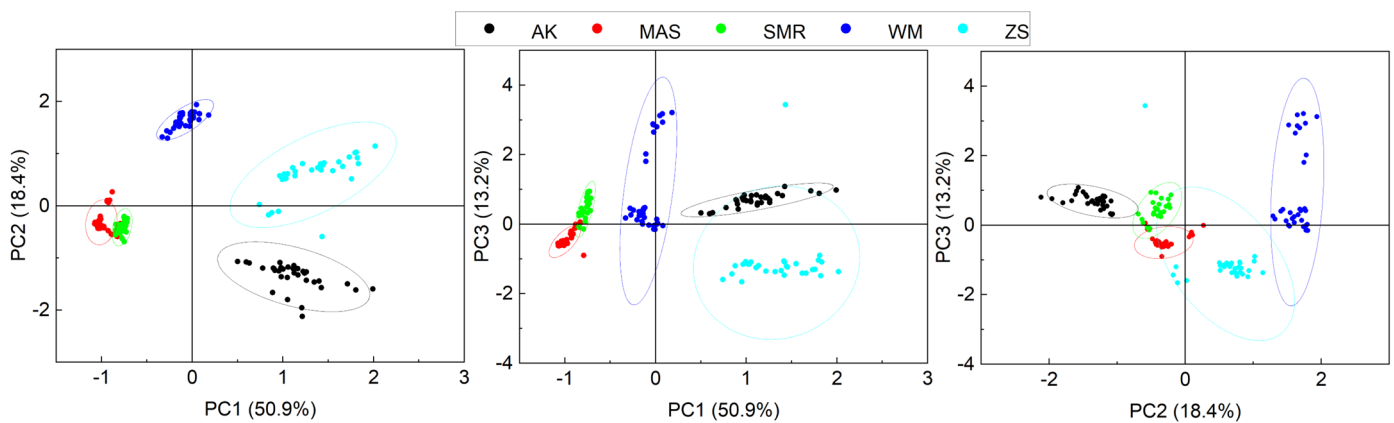


Figure 7. Principal component analysis results of 10 elemental variables after RF selection.

### 3.4. Linear Discriminant Analysis

In the origin discrimination model of turquoise, 56 elements are screened for variables, and whether the 56 variables entered the discrimination model was dependent on the p value (significance level) of the evaluation parameter. When  $p < 0.05$ , the variable is retained; when  $p \geq 0.05$ , the variable is excluded from the model. Finally, 48 elements that had a significant effect on origin discrimination are introduced into the discrimination model to establish five different origin recognition models of turquoise.

The canonical discriminant function F1, function F2, function F3, and function F4 can explain 36.8%, 33.4%, 19.0%, and 10.9% of the total variance variation, respectively, and the first three functions basically explain 89.1% of the total variance variation. Using F1, F2, and F3, it can be seen that the turquoise samples from different producing areas are a clear cluster, and only a few scattered points fall outside the cluster (Figure 8). The

turquoise in Zhushan, Mongolia, and Sleeping Beauty regions is clearly distinguished and the clustering effect is good. Among the F1 and F2 scatter, there are individual overlapping phenomena in the scattered points of the Ankang and Maanshan regions. This shows that the linear discrimination technology based on multi-element fingerprint information has a good ability to discriminate turquoise from different origins, and it is an effective method for origin traceability analysis.

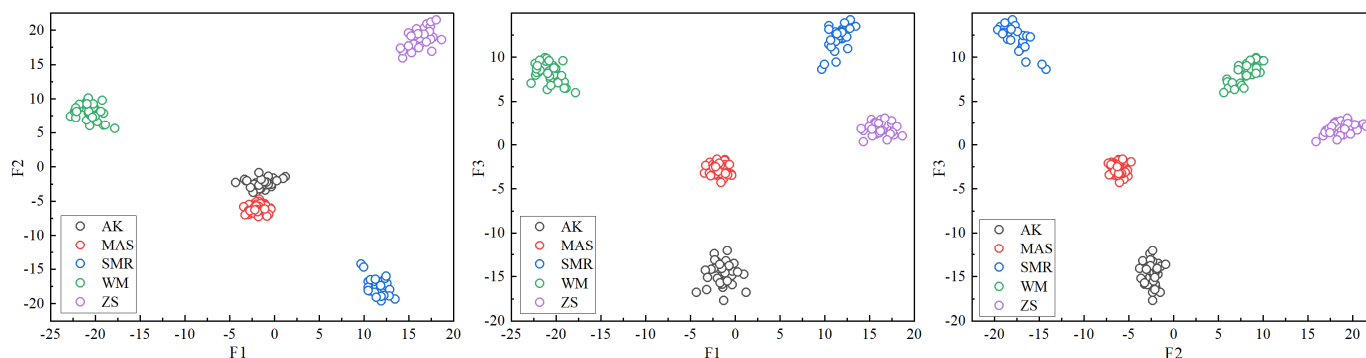


Figure 8. The canonical discriminant function diagram for different origins.

A cross-validation procedure was used to evaluate this model. A satisfactory classification was obtained, with an overall correct classification rate of 100% and a cross-validation rate of 99.5% (Table 3).

Table 3. Classification of turquoise samples from different regions.

|                 |       | Predicted Group Membership <sup>a</sup> |     |     |     |     |                    |       |
|-----------------|-------|---|-----|-----|-----|-----|--------------------|-------|
|                 |       |   | AK  | MAS | SMR | WM  | ZS                 | Total |
| Original        | Count | AK                                      | 33  | 0   | 0   | 0   | 0                  |       |
|                 |       | MAS                                     | 0   | 58  | 0   | 0   | 0                  |       |
|                 |       | SMR                                     | 0   | 0   | 26  | 0   | 0                  |       |
|                 |       | WM                                      | 0   | 0   | 0   | 33  | 0                  |       |
|                 |       | ZS                                      | 0   | 0   | 0   | 0   | 33                 |       |
|                 | %     |   | 100 | 100 | 100 | 100 | 100 <sup>b</sup>   |       |
| Cross-validated | Count | AK                                      | 33  | 0   | 0   | 0   | 0                  |       |
|                 |       | MAS                                     | 0   | 58  | 0   | 0   | 0                  |       |
|                 |       | SMR                                     | 0   | 0   | 26  | 0   | 0                  |       |
|                 |       | WM                                      | 0   | 0   | 0   | 33  | 0                  |       |
|                 |       | ZS                                      | 0   | 0   | 1   | 0   | 32                 |       |
|                 | %     |   |     |     |     |     | 99.5% <sup>c</sup> |       |

<sup>a</sup> Diagonally tabulated data show how many observations were successfully categorized. <sup>b</sup> Of empirical grouped observations, 100% were correctly classified. <sup>c</sup> Of cross-validated grouped observations, 99.5% were correctly classified.

This classification model could clearly discriminate samples from Ankang, Maanshan and Mongolia. In addition, there was an inaccurate prediction in the discrimination between Sleeping beauty and Zhushan. It shows that the recognition results of this discriminant model for five different producing areas are satisfactory.

#### 4. Conclusions

LA-ICP-MS is an effective tool for fingerprint microsampling analysis of turquoise elements. For the first time, under the condition of 48 elemental variables, the PCA plot of source areas is tightly grouped. With the help of random forest importance screening, the ability to distinguish the five producing areas has been greatly improved by the principal component analysis method. By taking 48 elements as characteristic variables and introducing them into the discriminant model, a Fisher discriminant model for identifying

the origin of turquoise was established. The effective element fingerprint information for turquoise species is closely related to their origins, and the accuracy of cross-validation is achieved. This demonstrates that it is feasible to use this model to identify the origin of turquoise samples.

**Supplementary Materials:** The following supporting information can be downloaded at: <https://www.mdpi.com/article/10.3390/min13101338/s1>; Table S1: Corresponding elemental composition in Figure 1.

**Author Contributions:** Investigation, S.T. and L.L.; methodology, S.T., G.C. and D.Z.; resources, S.T., W.Z. and S.Z.; experiments S.T., S.P., D.Z. and W.H.; Supervision, W.Z. and S.L.; writing—original draft, S.T.; writing—review and editing, S.T., S.L. and W.H. All authors have read and agreed to the published version of the manuscript.

**Funding:** This research was funded by National Natural Science Foundation of China (No. 42003017), National Key R&D Program of China (2021YFC2903005), Hubei Provincial Natural Science Foundation of China (2023AFB1104), the Research Fund Program of Key Laboratory of Gold Mineralization Processes and Resource Utilization, MNR and Shandong Provincial Key Laboratory of Metallogenic Geological Process and Resource Utilization (KFKT202112), and the Science and Technology Project of Hubei Geological Bureau (KJ2023-40, KJ2023-38-03 and KCDZ2023-22).

**Data Availability Statement:** Not applicable.

**Acknowledgments:** The authors would like to thank all the institutions listed in Funding section for their financial support.

**Conflicts of Interest:** The authors declare no conflict of interest.

## References

1. Nikbakht, T. Investigation of Turquoise Gemstone Using Micro-PIXE Imaging Technique. *Nucl. Instrum. Methods Phys. Res. Sect. B Beam Interact. Mater. At.* **2020**, *484*, 5–11. [CrossRef]
2. Taghipour, B.; Mackizadeh, M.A. The Origin of the Tourmaline-Turquoise Association Hosted in Hydrothermally Altered Rocks of the Kuh-Zar Cu-Au-Turquoise Deposit, Damghan, Iran. *Neues Jahrb. Für Geol. Und Paläontologie Abh.* **2014**, *272*, 61–77. [CrossRef]
3. Weigand, P.C.; Harbottle, G.; Sayre, E.V. Turquoise sources and source analysis: Mesoamerica and the southwestern U.S.A. *Exch. Syst. Prehistory* **1977**, *1*, 15–34. [CrossRef]
4. Fritsch, E.; McClure, S.F.; Ostrooumov, M.; Andres, Y.; Moses, T.; Koivula, J.I.; Kammerling, R.C. The Identification of Zachery-Treated Turquoise. *Gems Gemol.* **1999**, *35*, 4–16. [CrossRef]
5. Thibodeau, A.M.; Killick, D.; Hedquist, S.L.; Chesley, J.T.; Ruiz, J. Isotopic Evidence for the Provenance of Turquoise in the Southwestern United States. *Geol. Soc. Am. Bull.* **2015**, *127*, 1617–1631. [CrossRef]
6. Shirdam, B.; Shen, A.H.; Yang, M.; Mokhtari, Z.; Fazliani, H. Persian Turquoise: The Ancient Treasure of Neyshabur. *Gems Gemol.* **2021**, *57*, 240–257. [CrossRef]
7. Chen, Q.; Yin, Z.; Qi, L.; Xiong, Y. Turquoise from Zhushan County, Hubei Province, China. *Gems Gemol.* **2012**, *48*, 198–204. [CrossRef]
8. Zhang, Z.; Shen, A.-H. Fluorescence and Phosphorescence Spectroscopies and Their Applications in Gem Characterization. *Minerals* **2023**, *13*, 626. [CrossRef]
9. Othmane, G.; Hull, S.; Fayek, M.; Rouxel, O.; Lahd Geagea, M.; Kyser, T.K. Hydrogen and Copper Isotope Analysis of Turquoise by SIMS: Calibration and Matrix Effects. *Chem. Geol.* **2015**, *395*, 41–49. [CrossRef]
10. Hull, S.; Fayek, M.; Mathien, F.J.; Shelley, P.; Durand, K.R. A New Approach to Determining the Geological Provenance of Turquoise Artifacts Using Hydrogen and Copper Stable Isotopes. *J. Archaeol. Sci.* **2008**, *35*, 1355–1369. [CrossRef]
11. Consonni, R. Laura Ruth Cagliani Nuclear Magnetic Resonance and Chemometrics to Assess Geographical Origin and Quality of Traditional Food Products. *Adv. Food Nutr. Res.* **2010**, *59*, 87–165. [CrossRef] [PubMed]
12. Vitale, R.; Bevilacqua, M.; Bucci, R.; Magri, A.D.; Magri, A.L.; Marini, F. A Rapid and Non-Invasive Method for Authenticating the Origin of Pistachio Samples by NIR Spectroscopy and Chemometrics. *Chemom. Intell. Lab. Syst.* **2013**, *121*, 90–99. [CrossRef]
13. Tahir, H.E.; Arslan, M.; Mahunu, G.K.; Mariod, A.A.; Hashim, S.B.; Xiaobo, Z.; Jiyong, S.; El-Seedi, H.R.; Musa, T.H. The Use of Analytical Techniques Coupled with Chemometrics for Tracing the Geographical Origin of Oils: A Systematic Review (2013–2020). *Food Chem.* **2022**, *366*, 130633. [CrossRef]
14. Silva, C.S.; Borba, F.d.S.L.; Pimentel, M.F.; Pontes, M.J.C.; Honorato, R.S.; Pasquini, C. Classification of Blue Pen Ink Using Infrared Spectroscopy and Linear Discriminant Analysis. *Microchem. J.* **2013**, *109*, 122–127. [CrossRef]
15. Chen, X.; Xun, Y.; Li, W.; Zhang, J. Combining Discriminant Analysis and Neural Networks for Corn Variety Identification. *Comput. Electron. Agric.* **2010**, *71*, S48–S53. [CrossRef]

16. Gajek, M.; Pawlaczyk, A.; Szykowska-Jozwik, M.I. Multi-Elemental Analysis of Wine Samples in Relation to Their Type, Origin, and Grape Variety. *Molecules* **2021**, *26*, 214. [[CrossRef](#)]
17. Coetzee, P.P.; Steffens, F.E.; Eiselen, R.J.; Augustyn, O.P.; Balcaen, L.; Vanhaecke, F. Multi-Element Analysis of South African Wines by ICP–MS and Their Classification according to Geographical Origin. *J. Agric. Food Chem.* **2005**, *53*, 5060–5066. [[CrossRef](#)]
18. Soares, F.; Anzanello, M.J.; Fogliatto, F.S.; Caetano, M.; Ferrão, M.F.; Manfroi, V.; Pozebon, D. Element Selection and Concentration Analysis for Classifying South America Wine Samples according to the Country of Origin. *Comput. Electron. Agric.* **2018**, *150*, 33–40. [[CrossRef](#)]
19. Liu, X.; Zhao, Y.; Mu, J.; Zhang, J.; Zhang, A. Determination of Geographical Origin of Concentrated Apple Juice through Analysis of Stable Isotopic and Mineral Elemental Fingerprints: Preliminary Results. *J. Sci. Food Agric.* **2021**, *101*, 3795–3803. [[CrossRef](#)]
20. Liu, X.; Mu, J.; Tan, D.; Mao, K.; Zhang, J.; Sadiq, F.A.; Sang, Y.; Zhang, A. Application of Stable Isotopic and Mineral Elemental Fingerprints in Identifying the Geographical Origin of Concentrated Apple Juice in China. *Food Chem.* **2022**, *391*, 133269. [[CrossRef](#)]
21. von Wuthenau, K.; Segelke, T.; Kuschnerit, A.; Fischer, M. Glass Authentication: Laser Ablation-Inductively Coupled Plasma Mass Spectrometry (LA-ICP-MS) for Origin Discrimination of Glass Bottles. *Talanta* **2021**, *235*, 122686. [[CrossRef](#)]
22. Katsurada, Y.; Sun, Z.; Breeding, C.M.; Dutrow, B.L. Geographic Origin Determination of Paraíba Tourmaline. *Gems Gemol.* **2019**, *55*, 648–659. [[CrossRef](#)]
23. Luo, Z.; Yang, M.; Shen, A.H. Origin Determination of Dolomite-Related White Nephrite through Iterative-Binary Linear Discriminant Analysis. *Gems Gemol.* **2015**, *1*, 300–311. [[CrossRef](#)]
24. Su, Y.; Yang, M. Combining Rare Earth Element Analysis and Chemometric Method to Determine the Geographical Origin of Nephrite. *Minerals* **2022**, *12*, 1399. [[CrossRef](#)]
25. Zhang, Z.; Ye, M.; Shen, A.H. Characterisation of Peridot from China’s Jilin Province and from North Korea. *J. Gemmol.* **2019**, *36*, 436–446. [[CrossRef](#)]
26. Liu, Y.; Hu, Z.; Gao, S.; Günther, D.; Xu, J.; Gao, C.; Chen, H. In Situ Analysis of Major and Trace Elements of Anhydrous Minerals by LA-ICP-MS without Applying an Internal Standard. *Chem. Geol.* **2008**, *257*, 34–43. [[CrossRef](#)]
27. Lin, J.; Liu, Y.; Yang, Y.-H.; Hu, Z. Calibration and Correction of LA-ICP-MS and LA-MC-ICP-MS Analyses for Element Contents and Isotopic Ratios. *Solid Earth Sci.* **2016**, *1*, 5–27. [[CrossRef](#)]
28. Luo, T. LA-ICP-MS Imaging Analysis of Gem-Quality Tourmaline: A Novel Method for Direct Identification of Chromophore in Gemstone Samples. *At. Spectrosc.* **2022**, *44*, 1–7. [[CrossRef](#)]
29. Guillon, M.; Günther, D. Quasi “Non-Destructive” Laser Ablation-Inductively Coupled Plasma-Mass Spectrometry Fingerprinting of Sapphires. *Spectrochim. Acta Part B At. Spectrosc.* **2001**, *56*, 1219–1231. [[CrossRef](#)]
30. Su, Y.; Yang, M. A Multi-Strategy Linear Discriminant Analysis (LDA) Method Coupled with Laser Ablation Inductively Coupled Plasma Mass Spectrometry (LA-ICP-MS) for Discriminating the Geographical Origin of Nephrite. *J. Anal. At. Spectrom.* **2023**, *38*, 667–680. [[CrossRef](#)]
31. Bindereif, S.; Rüll, F.; Schwarzing, S.; Schwarzing, C. Chemometric Modeling of Trace Element Data for Origin Determination of Demantoid Garnets. *Minerals* **2020**, *10*, 1046. [[CrossRef](#)]
32. Wang, H.A.O.; Krzemnicki, M.S. Multi-Element Analysis of Minerals Using Laser Ablation Inductively Coupled Plasma Time of Flight Mass Spectrometry and Geochemical Data Visualization Using T-Distributed Stochastic Neighbor Embedding: Case Study on Emeralds. *J. Anal. At. Spectrom.* **2021**, *36*, 518–527. [[CrossRef](#)]
33. Carter, A.K.; Dussubieux, L. Geologic Provenience Analysis of Agate and Carnelian Beads Using Laser Ablation-Inductively Coupled Plasma-Mass Spectrometry (LA-ICP-MS): A Case Study from Iron Age Cambodia and Thailand. *J. Archaeol. Sci. Rep.* **2016**, *6*, 321–331. [[CrossRef](#)]
34. Pornwilard, M.-M.; Hansawek, R.; Shiowatana, J.; Siripinyanond, A. Geographical Origin Classification of Gem Corundum Using Elemental Fingerprint Analysis by Laser Ablation Inductively Coupled Plasma Mass Spectrometry. *Int. J. Mass Spectrom.* **2011**, *306*, 57–62. [[CrossRef](#)]
35. Resano, M.; Vanhaecke, F.; Hutsebaut, D.; De Corte, K.; Moens, L. Possibilities of Laser Ablation-Inductively Coupled Plasma-Mass Spectrometry for Diamond Fingerprinting. *J. Anal. At. Spectrom.* **2003**, *18*, 1238. [[CrossRef](#)]
36. Foord, E.E.; Taggart, J.E. A Reexamination of the Turquoise Group: The Mineral Aheylite, Planerite (Redefined), Turquoise and Coeruleolactite. *Mineral. Mag.* **1998**, *62*, 93–111. [[CrossRef](#)]
37. Liu, L.; Yang, M.; Liu, R.; He, C. Study on EDXRF Method of Turquoise Composition. *Spectrosc. Spectr. Anal.* **2018**, *38*, 1910–1916. [[CrossRef](#)]
38. Zhou, Q.; Wang, C.; Shen, A.H. Application of High-Temperature Copper Diffusion in Surface Recoloring of Faceted Labradorites. *Minerals* **2022**, *12*, 920. [[CrossRef](#)]
39. Wang, X.; Guo, Y. The Impact of Trace Metal Cations and Absorbed Water on Colour Transition of Turquoise. *R. Soc. Open Sci.* **2021**, *8*, 201110. [[CrossRef](#)]
40. Fei, H.; Fan, Z.; Wang, C.; Zhang, N.; Wang, T.; Chen, R.; Bai, T. Cotton Classification Method at the County Scale Based on Multi-Features and Random Forest Feature Selection Algorithm and Classifier. *Remote Sens.* **2022**, *14*, 829. [[CrossRef](#)]
41. Chavent, M.; Genuer, R.; Saracco, J. Combining Clustering of Variables and Feature Selection Using Random Forests. *Commun. Stat. Simul. Comput.* **2019**, *50*, 426–445. [[CrossRef](#)]

42. Menze, B.H.; Kelm, B.M.; Masuch, R.; Himmelreich, U.; Bachert, P.; Petrich, W.; Hamprecht, F.A. A Comparison of Random Forest and Its Gini Importance with Standard Chemometric Methods for the Feature Selection and Classification of Spectral Data. *BMC Bioinform.* **2009**, *10*, 213. [[CrossRef](#)] [[PubMed](#)]
43. Rodionova, O.Y.; Titova, A.V.; Pomerantsev, A.L. Discriminant Analysis Is an Inappropriate Method of Authentication. *TrAC Trends Anal. Chem.* **2016**, *78*, 17–22. [[CrossRef](#)]

**Disclaimer/Publisher's Note:** The statements, opinions and data contained in all publications are solely those of the individual author(s) and contributor(s) and not of MDPI and/or the editor(s). MDPI and/or the editor(s) disclaim responsibility for any injury to people or property resulting from any ideas, methods, instructions or products referred to in the content.